



Cite this: *RSC Adv.*, 2020, 10, 16886

Received 14th February 2020  
Accepted 13th April 2020

DOI: 10.1039/d0ra01437k

rsc.li/rsc-advances

# A two-dimensional crystal growth in anatase titania nanostructures driven by trigonal hydronium ions

Siti Khatijah Md Saad, Nabilah Alias, Muhamad Adam Ramli, Nur Adliha Abdullah, Nurul Ain Abd Malek, Mohd Mustaqim Rosli and Akrajas Ali Umar \*

Two-dimensional growth or high-energy faceting during a wet-chemical nanocrystal growth involves a dynamic surfactant functionalization that selectively allows a particular crystal plane to grow and simultaneously, passivates others from evolving. Here, by simply controlling the concentration of hydronium ions in a liquid-phase deposition reaction, the two-dimensional growth of a few atoms thick and (001) facet in anatase titania nanostructures can be achieved. The morphology can be modified from nanocube to nanobelt and nanosheet by increasing the hydronium ion concentration. Raman analysis reveals that the trigonal hydronium ions attach to the growing planes of anatase  $\text{TiO}_2$  via a dative bonding, projecting atom-thick and large-scale (001) faceted nanobelts and nanosheets.

## 1. Introduction

This study reports a facile strategy to promote a two-dimensional and (001) faceted growth in anatase titania by utilizing the unique chemistry of a trigonal pyramid skeleton of hydronium ions as directing agents in a simple liquid-phase deposition method. Two-dimensional nanostructures and (001) faceting in anatase titania nanostructures have been the focus of attention in the materials chemistry synthesis field due to their special properties with high surface energy that promise enhanced surface reactions, charge transfer, and physico-chemical processes on the surface.<sup>1–3</sup> In the anatase phase, the (001) facet is the second highest in surface energy after (110). The surface energy is  $0.90 \text{ J m}^{-2}$ , which is double that of the most stable facet (101), *i.e.*,  $0.44 \text{ J m}^{-2}$ .<sup>4–7</sup> Due to its unique surface atom coordination state with face-to-face Ti atoms, it has been anticipated that massive photocatalytic, photovoltaic, molecular dissolution or adsorption activities are expected to occur on this surface, thus making the production of anatase titania nanostructures with (001) facets highly desirable.<sup>2,3</sup> If (001) faceting is then combined with unique characteristics arising from the material with a few atoms thick or two-dimensional structures, the two-dimensional and (001) faceted titania nanostructures with unusual properties could be obtained.

Although its a lengthy growth reaction process that requires more than 10 h in a typical process, the liquid-phase deposition is a versatile method to grow a wide range of metal oxide complex films on a solid substrate from the hydrolysis of metal fluoro cation precursors.<sup>8–11</sup> Combining with a thermal

annealing phase refinement, a pure crystalline phase of a metal oxide nanostructure film can be obtained on the substrate surface. Though, in most cases, the metal oxide product on the substrate surface is simply a continuous thin film with an extensively cracked structure, which occurs due to high surface tension. By controlling the reaction conditions such as concentration and temperature, irregular shape nanoparticle thin films can normally be obtained, and by changing the fluoride scavenger in the reaction, the growth process can be accelerated to below 5 h. In a recent study, we found that by increasing the number of fluoride ions liberated during the reaction, a hierarchical structure of a few tens of micrometers in a lateral size composed of a (001) faceted nanocuboid was realized.<sup>9,12–14</sup> In order to take advantage of the low-dimensional properties of materials, the nanometer scale of anatase titania with the dominant (001) faceting should be realized.

Contrary to its promising properties, the preparation of (001) faceted anatase  $\text{TiO}_2$  is challenging because of its thermodynamically unstable morphology, and the facet can easily turn into a highly stable (101) facet at a relatively low-growth temperature. Recently, a wide range of efforts have been dedicated to developing a systematic approach to achieve anatase titania nanostructures with the (001) facet in forms such as nanocubes or nanoplates. Fluorination methods, involving the use of a high amount of fluoride ions during the chemical growth process, such as HF,  $\text{NH}_4\text{F}$ , NaF,  $\text{NaBF}_4$ , and [bmim]- $[\text{BF}_4]$ , are the most favored approaches used so far.<sup>15–21</sup> In a typical process, the approach takes the advantage of fluoride ions', which are liberated in the reaction, preferred adsorption onto the growing (001) facet and then preserves it. Despite its efficient function in (001) faceting, in most cases, the fluorination effect is restricted only to the realization of titania nanostructures with a lateral dimension of not more than one

Institute of Microengineering and Nanoelectronics, Universiti Kebangsaan Malaysia, 43600, Bangi, Selangor, Malaysia. E-mail: akrajas@ukm.edu.my



micrometres. In addition, the nanostructure thickness is normally high, *i.e.*, up to several hundreds of nanometers, which make them lose precious properties resulting from the quantum effect. Therefore, a simple approach that may realize the (001) faceted titania nanostructures with a lateral dimension in a few tens of micrometres but with a few nanometres or atoms thick is highly desirable for better functionalization and a broader spectrum of applications.

Here, we demonstrated that ultra-thin, a few atoms thick nanosheet structure of anatase can be realized *via* a controlled two-dimensional crystal growth in a simple liquid-phase deposition reaction under a high concentration of a fluoride scavenger. We discovered that the hydronium ions, trigonal pyramid species generated during the hydrolysis of a boric acid fluoride scavenger in a liquid-phase deposition reaction of titania complexes are the key agents in driving the (001) faceting and two-dimensional crystal growth of the anatase titania nanostructures. Raman analysis indicated that these ions actively form a dative bonding with Ti atomic sites on the (001) facet and projects a two-dimensional crystal growth of a few atoms thick and (001) faceting of anatase titania nanostructures. The ultra-thin (001) faceted titania nanosheets should find extensive application in catalysis, solar cells and sensors.

## 2. Experimental

### 2.1 Materials

For the preparation of the (001) faceted and ultra-thin TiO<sub>2</sub> nanosheets, two chemical reagents were used, namely potassium hexafluorotitanate (KTiF<sub>6</sub>) (99.9%) and boric acid (H<sub>3</sub>BO<sub>3</sub>) (99.5%). Both chemicals were purchased from Sigma-Aldrich, USA. KTiF<sub>6</sub> functioned as the metal oxide precursor, while H<sub>3</sub>BO<sub>3</sub> was used as a fluoride scavenger in the reaction. All the chemicals were used as-received and without any further purification process. The solutions of all the chemicals were prepared using pure water (approximately 18.2 MΩ) that was obtained from a Merck Milipore Milli-Q (Finland) water purification system. Moreover, an ITO substrate (~9 Ω per square) was purchased from Kaivo Instrument (China) and cut into 1.0 × 1.5 cm dimension.

### 2.2 Synthesis of ultrathin TiO<sub>2</sub> nanosheets

Anatase titania nanostructures were prepared on top of the ITO substrate *via* a liquid phase deposition<sup>22</sup> method involving the hydrolysis of a metal-fluoro cation, namely potassium hexafluorotitanate (KTiF<sub>6</sub>) and boric acid (H<sub>3</sub>BO<sub>3</sub>), as a fluoride scavenger. The ITO substrate was cleaned *via* an ultrasonication process for 15 min each with pure water, acetone, and ethanol prior to the growth process. The clean substrate was then vertically hung in a 20 mL glass vial. In a typical synthesis process, 5 mL of 0.1 M aqueous potassium hexafluorotitanate, KTiF<sub>6</sub> was heated in a water bath at a temperature of 90 °C, prior to the addition of 5 mL of 0.1 M H<sub>3</sub>BO<sub>3</sub>. The mixed solution was kept in a water bath for 30 min at a temperature of 90 °C. During the growth process, the color of the solution changed from

colorless to a white and cloudy solution. After 30 min, a white-coloured layer of the thin film could be observed on top of the ITO substrate, an indication of the growth of a titania complex nanostructure film on the surface of the substrate. The sample was then annealed in air at 400 °C for 1 h.

### 2.3 Characterizations of nanostructures

The morphology of the samples was examined *via* a field emission scanning electron microscope (FESEM, Zeiss Merlin Compact 55 kV). The microscope was supported by an Aztec energy dispersive spectroscopy apparatus for the elemental analysis. The analysis of phase crystallinity and faceting in the samples was carried out *via* X-ray diffraction technique on a Bruker D8 Advance instrument, with CuKα radiation ( $\lambda = 1.5 \text{ \AA}$ ) at a scan rate of  $2^\circ \text{ min}^{-1}$ . Raman spectroscopy was performed to examine the chemistry of the nanostructures, particularly the surface-ligand coordination, using a CRM 200 Witex Raman spectrometer with a 532 nm excitation laser.

## 3. Results and discussion

We carried out the FESEM analysis of the as-prepared samples and found that the morphology of titania nanostructures changes from a flower-like shape to a cubic shape when the

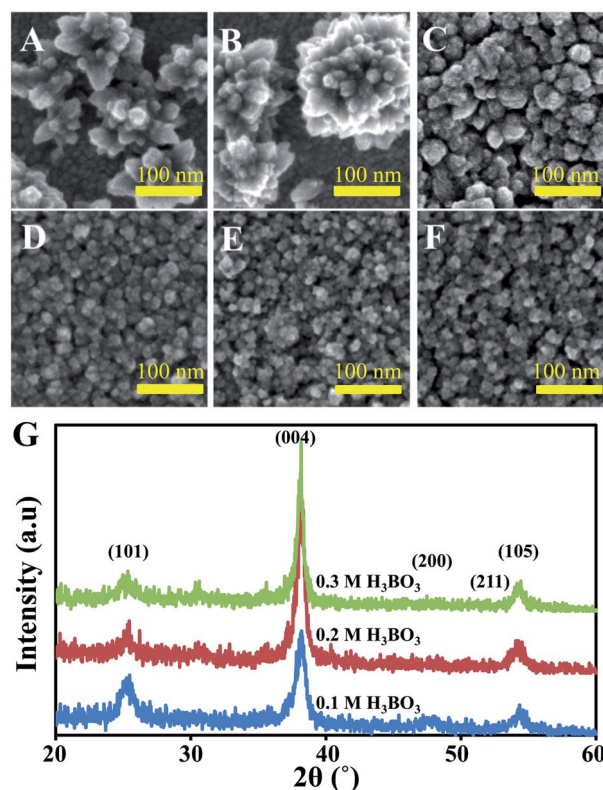


Fig. 1 Morphological and phase crystallinity properties of anatase TiO<sub>2</sub> prepared using KTiF<sub>6</sub>. An anatase TiO<sub>2</sub> nanoparticle thin film prepared using H<sub>3</sub>BO<sub>3</sub> at six different concentrations of (A) 0.025, (B) 0.05, (C) 0.1, (D) 0.2, (E) 0.3 and (F) 0.5 M. (G) XRD spectra of the anatase TiO<sub>2</sub> nanoparticle thin film prepared using H<sub>3</sub>BO<sub>3</sub> at concentrations of 0.1, 0.3 and 0.5 M. Scale bars are 100 nm.

concentration of boric acid increased from 0.025 to 0.5 M (Fig. 1). Regarding the nanocube sample, prepared at boric acid concentrations between 0.3 and 0.5 M, the typical edge-length was approximately  $20 \pm 3$  nm. Due to their high surface energy, the nanocubes tend to attach to one another, forming a clustered or networked nanocube film, which in turn homogeneously covers the entire surface of the substrate (see Fig. 1F). However, there were no significant modifications in the dimensions of the nanocubes when the concentration of boric acid was increased in the reaction (Fig. 1F). While FESEM analysis provided the isolated area characterization of titania nanostructures on the surface, XRD spectra further revealed the general structural information of the titania nanostructures prepared under different concentrations of boric acid, that is the structure wrapped by the (001) facet (Fig. 1G) as revealed by the peak intensity ratio between (004) and (101) planes. As can be seen from Fig. 1G, for the anatase titania prepared under different boric acid concentrations, the intensity of X-ray diffraction for the Bragg plane of (004) increases with the increase in the concentration of boric acid. On the contrary, the diffraction peak at the (101) Bragg plane decreases with the increase in the boric acid concentration. We calculated that the intensity ratio between (004) and (101) planes is from approximately 2 to 5 when the boric acid concentration is increased from 0.1 to 0.3 M. In normal non-faceted anatase nanostructures with a dominant (101) plane, this ratio is around 0.1 to 0.3. Because the (004) plane is equivalent to the (001) plane, it may be worth to mentioning that increasing the boric acid concentration in the reaction mixture has efficiently produced nanostructured titania with morphology enwrapped by (001) facet.

When the concentration was further increased, for example, to 0.6 M, titania nanostructures with a belt-like morphology were obtained (Fig. 2A and B). The nanobelt dimensions increased with the increase in the boric acid concentration. The

typical length of nanobelts prepared at 0.65 M is  $3 \pm 1.5$   $\mu\text{m}$  and can be up to tens of micrometres (Fig. 2B), with a width of  $15 \pm 3$  nm. Meanwhile, the thickness is approximately  $5 \pm 1.5$  nm and many of them can be down to a few atoms thick (Fig. 2D), making them ultrathin titania nanobelts produced so far. We carried out the high-resolution transmission microscopy (HRTEM) and selected area electron diffraction (SAED) analysis on these ultra-thin nanobelts to verify the thickness and faceting of the ultra-thin structures. The fact that the amorphous background of the carbon film can be seen in detail through the nanobelt structure indicates that the thickness of the nanosheets could be a few atoms thick. HRTEM also further shows that the nanobelts are single crystalline in nature with the exposed facet belonging to the (001) plane (see Fig. 2D and E). Unfortunately, the nature of the two-dimensional growth of titania at a boric acid concentration higher than 0.65 M cannot be observed due to the insolubility issue.

In addition to this massive nanobelt formation at high boric acid concentrations, we also noticed the projection of ultrathin nanosheet structures of titania (see the dashed square in Fig. 3), which is indicated by a cloudy white part in the image (Fig. 3A) and pointed out by the red arrow in Fig. 3B. This ultra-thin structure was observed on the entire surface of the nanobelt structure. Considering the highly transparent nature of the nanosheets to the electron beam, which is indicated by the clear background substrate image seen through the electron beam (Fig. 3B) and its similarity to the nanobelt structures as shown in Fig. 2D, the nanosheets could also be a few atoms thick structures. Unfortunately, due to the limitations of the technique, the exact thickness of the ultra-thin nanosheets could not be accessed. By transferring the nanosheets onto a TEM grid, we analysed the surface properties of the ultra-thin nanosheet structures. Fig. 3C and D show that the ultra-thin nanosheets along with the nanobelt structures have been

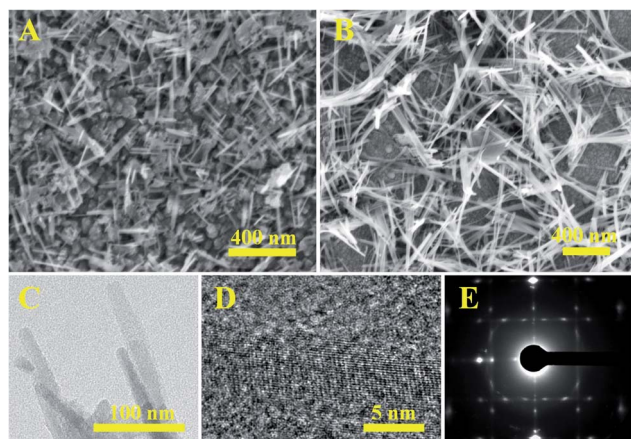


Fig. 2 Morphological and crystallinity properties of the 2D anatase  $\text{TiO}_2$  nanobelts. The FESEM images of titania nanobelts prepared using boric acid concentrations of 0.6 (A) and 0.65 M (B). The corresponding TEM images (C–E) of the  $\text{TiO}_2$  nanobelt samples of (B). (D and E) The typical high-resolution TEM images and selected area diffraction (SAED) of the  $\text{TiO}_2$  nanobelts, respectively.

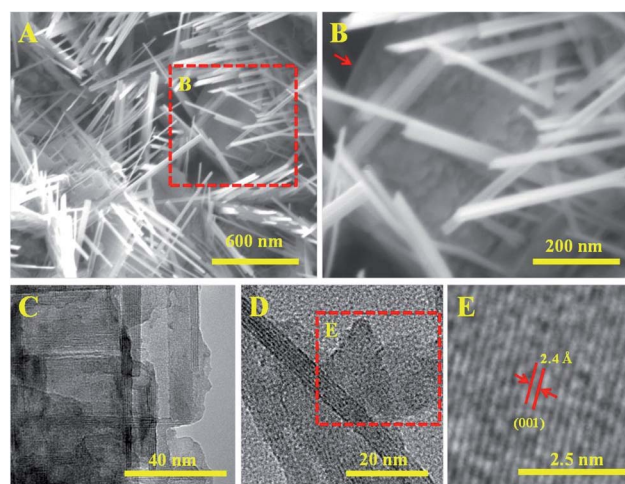


Fig. 3 A few atoms thick two-dimensional nanosheets of titania. (A) and (B) show the FESEM images of titania nanosheets grow along with the nanobelt structures of titania. (C and D) Low resolutions the TEM images of nanosheets. Red-dashed square in (D) points out typical few atoms thick nanosheets. (E) is a high-resolution TEM image of nanosheets showing the (001) facet.

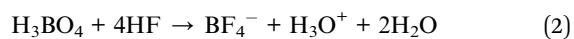
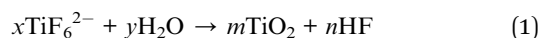




successfully transferred onto the TEM grid. However, the nanosheets observed on the TEM grid are not as thin as the one shown in Fig. 3B. Nevertheless, similar to the nanobelt structures, the high-resolution TEM analysis also reveals that the nanosheets are characterized by the (001) facet (Fig. 3E). This fact certainly provides a clear view of the simplicity of the present method in promoting the growth of atomically thin two-dimensional structures of anatase TiO<sub>2</sub>. Thus, exceptional performance in solar cells, catalysis, sensing, and optoelectronic applications are expected when such ultra-thin anatase TiO<sub>2</sub> nanosheets are used.

Although interesting structural properties of titania nanostructures have been obtained on materials prepared using the present approach, so far their exact formation mechanism is still not well-understood. However, we summarize the following facts: (i) the titania nanocube is formed by using a boric acid concentration in the range of 0.2 and 0.3 M. If a lower concentration is used, the morphology is varied from a flower-like shape to an irregular shape nanoparticle film. Meanwhile, if the concentration is higher than 0.3 M, the nanostructure product becomes ultra-thin nanobelt structures. (ii) The temperature should be 90 °C to facilitate a controlled growth process. A lower growth temperature produces titania nanostructures with an irregular shape. Their size is also relatively big as a result of the low kinetic growth process. Unfortunately, a higher growth temperature of above 90 °C cannot be obtained due to the boiling of the reaction mixture at this temperature, leading to the uncontrolled growth of nanocrystals.

Nevertheless, as has been noted earlier in this study, we hypothesize that the effect of hydronium ion passivation on the titania nanostructure surface could be the driving factor for the realization of (001) faceting in the anatase titania. The existence of an excess amount of boric acid liberates a high amount of hydronium (H<sub>3</sub>O<sup>+</sup>) ions in the reaction. Owing to their strong Lewis acid character,<sup>23</sup> they can be easily adsorbed onto the growing crystal plane and passivated them. Since their molecular structure is a trigonal pyramid, they are easily oriented with the flat surface for efficient surface passivation, projecting a two-dimensional crystal growth. In order to simplify the assumption, the following process is considered: in a liquid-phase deposition reaction, the metal fluoro cation complexes were hydrolyzed by water molecules producing a Ti complex and fluoride anions. The fluoride ions may then be captured by boric acid, forming BF<sub>4</sub><sup>-</sup> and hydronium ions.<sup>24</sup> The reaction is given by:<sup>22</sup>



for metal complex (1) and boric acid (2) hydrolysis, respectively, where  $x$ ,  $y$ ,  $m$  and  $n$  in (1) are the molarity coefficients of the reaction. If the concentration ratio between the boric acid and the fluoride ion byproduct is balanced, a continuous metal oxide complex layer will be formed on any solid substrate surface. Moreover, in the case of fluoride ions being abundantly available in the reaction due to the lack of a fluoride ion

scavenger, they will tend to bind to the growing plane of titania *via* either Ti-F or Ti-O-F coordination. This phenomenon will passivate the expansion of that plane, producing titania complex nanostructures with a platonic morphology, particularly cuboid structures. In a normal case, the coordination of fluoride ions with the crystal plane of the titania complex is on the (001) facet. This case is more or less similar to the fluoridation effect during the synthesis of (001) faceted titania nanostructures.<sup>25</sup> As a result, nanostructures with a dominant and large area of the (001) plane are produced. When fluoride ion concentration is relatively high in the reaction, nanocuboids with a size of few nanometers are produced. Due to their high surface energy, they rearrange and stack with each other, forming a hierarchical porous micrometer nanoplate structure.<sup>13</sup> In the opposite case, where the fluoride scavenger, *i.e.* boric acid, is far exceeding the concentration of fluoride ions in the reaction, the boric acid will be hydrolyzed forming higher borate species and hydronium ions (H<sub>3</sub>O<sup>+</sup>). While borate is chemically relatively stable residing in the bulk of the solution and can be further reduced to a lower borate species when reacting again with hydronium ions, as mentioned earlier, the hydronium ions with relatively smaller molecular size are reactive and will quickly attach onto the surface of a titania complex growing planes *via* an electron-donating process, forming a dative bond. With its unique molecular structure of trigonal pyramid symmetry, the hydronium ion can easily re-oriented parallel to the surface of the titania complex plane, facilitating efficient passivation for (001) faceting and promoting two-dimensional crystal growth process in the titania nanostructures.

In order to verify this aspect, we carried out Raman spectroscopy on the sample, and the results are shown in Fig. 4. As can be seen from the figure, at least two Raman vibration modes related to hydronium ion (H<sub>3</sub>O<sup>+</sup>), *i.e.* at the wavenumbers of 3000 to 3670 cm<sup>-1</sup>, are seen in the spectrum.<sup>26,27</sup> Meanwhile, the coordination of hydronium molecules with the surface is facilitated by the dative bond Ti-O-H at the wavenumbers of 250 and 541.5 cm<sup>-1</sup> as reported in an earlier study.<sup>28</sup> It is well known that fluorine is also liberated during the hydrolysis of KTiF in which, in many cases, it plays a critical role in the (001) faceting of anatase TiO<sub>2</sub>, but it does not show a capability to promote the two-dimensional crystal growth. In this study, the occurrence of the fluoridation process is judged *via* EDX analysis results. However, considering that the existence of fluoride on the surface of the TiO<sub>2</sub> nanosheet/nanobelt samples cannot be detected *via* Raman spectroscopy, its role could be simply to project the (001) faceting on the anatase TiO<sub>2</sub> nanostructures. Furthermore, it is also observed that the potassium cations (K<sup>+</sup>) are incorporated into the anatase nanostructured sample, but its amount is relatively low as judged from the EDX elemental analysis. Because the XRD analysis does not show any modification of the anatase crystalline phase, we believe that the K<sup>+</sup> ion should only be an impurity in the nanocrystals. Thus, it should not contribute to the promotion of the two-dimensional crystal growth. This assumption is likely valid as the K<sup>+</sup> ion impurities were only found to induce one-dimensional growth in titania nanostructures, producing a nanorod morphology, as reported in the



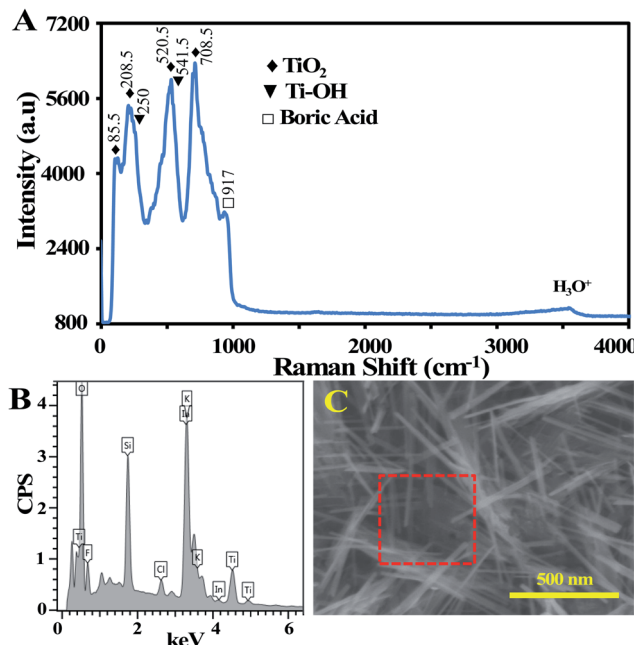


Fig. 4 Surface chemical coordination and elemental properties of 2D anatase TiO<sub>2</sub> (nanosheets and nanobelts). (A) Raman spectrum, (B) EDX spectrum and (C) a corresponding FESEM micrograph where the EDX analysis was taken (red dashed square), showing nanobelts and nanosheets (whitish overlayer, as in Fig. 3B) structures. The nanosheet structure is very transparent because of using 15 kV electron acceleration potential for the EDX analysis, leaving the nanosheets as a whitish overlayer only on the entire image (C).

recent literature.<sup>29–31</sup> On the basis of these facts, it can be confirmed that the hydronium ions' surface passivation effect is the key aspect for the formation of the two-dimensional structure. A combination effect with the surface fluoridation process, the (001) faceted two-dimensional anatase TiO<sub>2</sub> nanostructure is realized.

## 4. Conclusions

To conclude, it is remarked that efficient two-dimensional growth and (001) faceting in anatase titania nanostructures can be easily achieved *via* the effect of trigonal hydronium ion passivation. The hydronium ions were generated during the liquid-phase deposition *via* the hydrolysis of boric acid (as a fluoride scavenger) if their concentration is far higher than the fluoride ions liberated during the hydrolysis of the metal-fluoro cation. The growth process is rapid and only required 30 min to grow a large-scale of anatase titania nanosheets or nanobelts-constructed films on the surface of the substrate. The nanobelts and nanosheets of titania could be a few atoms thick that may produce unusual optoelectrical properties for potential applications in photocatalysis, dye-sensitized solar cells, and optoelectronic applications.

## Conflicts of interest

The authors declare that they have no conflict of interest.

## Acknowledgements

The authors are grateful for financial support from Universiti Kebangsaan Malaysia under GUP-2018-083 and MI-2019-001 grants and the Ministry of Higher Education of Malaysia under FRGS/1/2019/STG02/UKM/02/3 grant.

## References

- 1 Y. Zhang, F. Fu, F. Zhou, X. Yang, D. Zhang and Y. Chen, *Appl. Surf. Sci.*, 2020, **510**, 145451.
- 2 Y. Zhu, Z. Zhang, N. Lu, R. Hua and B. Dong, *Chin. J. Catal.*, 2019, **40**, 413–423.
- 3 W.-Y. Zhou, J.-Y. Liu, J.-Y. Song, J.-J. Li, J.-H. Liu and X.-J. Huang, *Anal. Chem.*, 2017, **89**, 3386–3394.
- 4 O. Game, T. Kumari, U. Singh, V. Aravindan, S. Madhavi and S. B. Ogale, *Energy Storage Materials*, 2016, **3**, 106–112.
- 5 N. Roy, Y. Sohn and D. Pradhan, *ACS Nano*, 2013, **7**, 2532–2540.
- 6 Y. Liao, H. Zhang, W. Que, P. Zhong, F. Bai, Z. Zhong, Q. Wen and W. Chen, *ACS Appl. Mater. Interfaces*, 2013, **5**, 6463–6466.
- 7 W. Wei, N. Yaru, L. Chunhua and X. Zhongzi, *RSC Adv.*, 2012, **2**, 8286–8288.
- 8 A. Y. A. Al-She'irey, S. K. M. Saad, A. A. Umar, M. Y. A. Rahman and M. M. Salleh, *J. Alloys Compd.*, 2016, **674**, 470–476.
- 9 A. A. Umar, S. Nafisah, S. K. M. Saad, S. T. Tan, A. Balouch, M. M. Salleh and M. Oyama, *Sol. Energy Mater. Sol. Cells*, 2014, **122**, 174–182.
- 10 A. A. Umar, M. Y. A. Rahman, S. K. M. Saad, M. M. Salleh and M. Oyama, *Appl. Surf. Sci.*, 2013, **270**, 109–114.
- 11 A. A. Umar, M. Rahman, S. K. M. Saad and M. M. Salleh, *Int. J. Electrochem. Sci.*, 2012, **7**, 7855–7865.
- 12 A. A. Umar, S. K. M. Saad, M. I. A. Umar, M. Y. A. Rahman and M. Oyama, *Opt. Mater.*, 2018, **75**, 390–430.
- 13 S. K. Md Saad, A. Ali Umar, M. I. Ali Umar, M. Tomitori, M. Y. A. Rahman, M. Mat Salleh and M. Oyama, *ACS Omega*, 2018, **3**, 2579–2587.
- 14 S. K. M. Saad, A. A. Umar, H. Q. Nguyen, C. F. Dee, M. M. Salleh and M. Oyama, *RSC Adv.*, 2014, **4**, 57054–57063.
- 15 Y. Wang, Q. Hou, M. Ju and W. Li, *Nanomaterials*, 2019, **9**, 647.
- 16 Z. Lai, F. Peng, Y. Wang, H. Wang, H. Yu, P. Liu and H. Zhao, *J. Mater. Chem.*, 2012, **22**, 23906–23912.
- 17 X. Wang, G. Liu, L. Wang, J. Pan, G. Q. M. Lu and H.-M. Cheng, *J. Mater. Chem.*, 2011, **21**, 869–873.
- 18 W. Wang, C. Lu, Y. Ni and Z. Xu, *CrystEngComm*, 2013, **15**, 2537–2543.
- 19 X.-L. Cheng, M. Hu, R. Huang and J.-S. Jiang, *ACS Appl. Mater. Interfaces*, 2014, **6**, 19176–19183.
- 20 Y. Cao, L. Zong, Q. Li, C. Li, J. Li and J. Yang, *Appl. Surf. Sci.*, 2017, **391**, 311–317.
- 21 S. Han, Q. Niu, N. Qin, X. Gu, Y. Zhang and G. Zhao, *Chem. Commun.*, 2020, **56**, 1337–1340.
- 22 S. Deki, N. Yoshida, Y. Hiroe, K. Akamatsu, M. Mizuhata and A. Kojinami, *Solid State Ionics*, 2002, **151**, 1–9.
- 23 H. L. Clever, *J. Chem. Educ.*, 1963, **40**, 637.



- 24 S. K. M. Saad, A. A. Umar, M. Y. A. Rahman and M. M. Salleh, *Appl. Surf. Sci.*, 2015, **353**, 835–842.
- 25 Y. Wang, H. Zhang, Y. Han, P. Liu, X. Yao and H. Zhao, *Chem. Commun.*, 2011, **47**, 2829–2831.
- 26 P. A. Giguere and J. Guillot, *J. Phys. Chem.*, 1982, **86**, 3231–3233.
- 27 J. Mullhaupt and D. Hornig, *J. Chem. Phys.*, 1956, **24**, 169.
- 28 Y. Jing, H. Wang, J. Zhao, H. Yi and X. Wang, *Appl. Surf. Sci.*, 2015, **347**, 499–504.
- 29 X. Sun, X. Chen and Y. Li, *Inorg. Chem.*, 2002, **41**, 4996–4998.
- 30 J. Fan, Z. Li, W. Zhou, Y. Miao, Y. Zhang, J. Hu and G. Shao, *Appl. Surf. Sci.*, 2014, **319**, 75–82.
- 31 S.-O. Kang, H.-S. Jang, K.-B. Kim, B. H. Park, M.-J. Jung and Y.-I. Kim, *Mater. Res. Bull.*, 2008, **43**, 996–1003.

